2/13/2012

Resistive Wall Heating Due to Image Current on the Beam Chamber for a Superconducting Undulator

S.H. Kim, ASD MD Group

1. Introduction

The image-current heating on the resistive beam chamber of a superconducting undulator (SCU) was calculated based on the normal and anomalous skin effects [1-4]. Using the bulk resistivity of copper for the beam chamber, the heat loads were calculated for the residual resistivity ratios (RRRs) of unity at room temperature to 100 K at a cryogenic temperature as the reference. Then, using the resistivity of the specific aluminum alloy 6053-T5, which will be used for the SCU beam chamber, the heat loads were calculated [5].

An electron beam stored in a storage ring induces an image current on the inner conducting wall, mainly within a skin depth, of the beam chamber. The image current, with opposite charge to the electron beam, travels along the chamber wall in the same direction as the electron beam. The average current in the storage ring consists of a number of bunches. When the pattern of the bunched beam is repeated according to the rf frequency, the beam current may be expressed in terms of a Fourier series. The time structure of the image current is assumed to be the same as that of the beam current.

For a given resistivity of the chamber inner wall, the application of the normal or anomalous skin effect will depend on the harmonic numbers of the Fourier series of the beam current and the temperature of the chamber.

For a round beam chamber with a radius r, much larger than the beam size, one can assume that the image current density as well as the density square, may be uniform around the perimeter $2\pi r$. For the SCU beam chamber, which has a relatively narrow vertical gap compared to the width, the effective perimeter was estimated since the heat load should be proportional to the inverse of the perimeter.

2. Circulating Electron Beam

The time structure of the circulating beam current is expressed as

$$I_b(t) = I_{av} \sum_{n=-\infty}^{\infty} \lambda\left(t - n\frac{T_0}{M}\right), \tag{1}$$

where I_{av} is the average beam current, λ is the beam bunch, M is the number of equally spaced beam bunches, and T_0 is the revolution period:

$$\omega_0 = 2\pi f_0 = 2\pi \frac{1}{T_0} \text{ and } f_0 = 271.554 \cdot (kHz).$$

If one assumes a Gaussian distribution of the beam bunch in the longitudinal direction with σ_t as the RMS bunch length in the unit of time:

$$\lambda\left(t - n\frac{T_0}{M}\right) = \frac{1}{\sqrt{2\pi}\sigma_t} \exp\left(-\frac{(t - nT_0/M)^2}{2\sigma_t^2}\right),$$

the Fourier series of Eq. (1) may be expressed as

$$I_b(\omega) = I_{av}\frac{\omega_0}{2\pi}\exp[-\frac{(\omega\sigma_t)^2}{2}]\sum_{n=-\infty}^{\infty}\delta(\omega - nM\omega_0). \tag{2}$$

3. Normal Skin Effect

When the induced image current attenuates at a distance d from the inner wall of the chamber as $exp(-d/\delta_s)$, the well-known harmonic skin depth δ_s is defined as

$$\delta_s = \sqrt{\frac{2\rho}{\omega\mu_0}}, \tag{3}$$

where ρ is the bulk resistivity of the inner-wall material and μ_0 is the vacuum permeability assuming that the inner wall is nonmagnetic. The surface resistance (per unit surface area) for the image current parallel to the surface depends on the angular frequency and resistivity as

$$R_s(\omega) = \frac{\rho}{\delta_s} = \sqrt{\frac{\omega\mu_0\rho}{2}}. \tag{4}$$

The surface wall resistance for a beam pipe with a length L and an inner radius r is given by

$$R_s^{wall}(\omega) = \frac{L}{2\pi r}R_s(\omega) \tag{5}$$

From Eq. (2) and Eq. (5) the resistive wall heating per unit length may be calculated:

$$\begin{aligned}\frac{Ps}{L} &= \int[I_b(\omega)]^2\frac{1}{2\pi r}R_s(\omega)d\omega \\ &= 2I_{av}{}^2\frac{1.225}{2\pi r}\left(\frac{\mu_0\rho(B,T)}{2}\right)^{1/2}\frac{1}{M\omega_0\sigma_t^{3/2}},\end{aligned} \tag{6}$$

where $\rho(B,T)$ under a magnetic field B is given by Koehler's rule

$$\rho(B,T) = \rho(0,T)\left(1+10^{1.055\cdot\log(B\cdot RRR)-2.69}\right).$$

The wall heating may also be calculated by

$$\frac{Psn}{L} = 2I_{av}{}^2\frac{1}{2\pi r}\sum_{n=1}^{n_{max}}R_s(nM\omega_0)\exp[-(nM\omega_0\sigma_t)^2], \tag{7}$$

or a part of it may be calculated by choosing a set of limits on the summation.

4. Anomalous Skin Effect

Typically at a reduced resistivity at cryogenic temperatures, the skin depth becomes smaller than the electron mean free path. Then, only a fraction of the conduction

electrons moving almost parallel to the chamber surface is effective in carrying the current, which limits the effective conductivity of the wall. The surface resistance under the anomalous skin effect is given by [1-4]

$$R_{as}(\omega) = R_{\infty}(1+1.157\alpha^{-0.276}) \qquad \text{for } \alpha \geq 3 \qquad (8)$$

where R_{∞} is the surface resistance in the extreme anomalous region $\alpha \gg 1$ with ℓ as the electron mean free path in the chamber wall:

$$R_{\infty} = \left(\frac{\sqrt{3}}{16\pi}\rho\ell(\omega\mu_0)^2\right)^{\frac{1}{3}}, \qquad (9)$$

and the parameter α is given by

$$\alpha = \frac{3}{4}\omega\mu_0(\rho\ell)^2\rho^{-3}. \qquad (10)$$

Using the $\rho\ell$ data specifically for copper,

$$\rho\ell = 6.6\times10^{-16}(\Omega m^2), \qquad (11)$$

Eq. (9) may be simplified as

$$R_{\infty} = 1.123\times10^{-3}\left(\frac{\omega}{2\pi}\times10^{-9}\right)^{2/3}, \qquad (12)$$

and $\ell/\delta_s > \sqrt{2}$ for $\alpha > 3$.

Then, from Eq. (2) and Eq. (8) the resistive wall heating per unit length may be calculated as

$$\frac{Pas}{L} = \int[I_b(\omega)]^2\frac{1}{2\pi r}R_{as}(\omega)d\omega \qquad (13)$$

or

$$\frac{Pasn}{L} = 2I_{av}{}^2\frac{1}{2\pi r}\sum_{n=1}^{n_{\max}}R_{as}(nM\omega_0)\exp[-(nM\omega_0\sigma_t)^2]. \qquad (14)$$

5. Beam Chamber Cross Section

The image current density, in a round beam chamber with a radius much larger than the beam size, may be assumed to be uniform around the perimeter. As shown in Fig. 1 the cross section of the SCU beam chamber is quite wide compared to the vertical aperture $2h$. The distribution of the induced current density may be expressed as [6]

$$j(x) = \frac{1}{\cosh(x/h)}. \qquad (15)$$

From Eq. (15) j and j^2 are plotted in Fig. 2. The effective perimeters, calculated from the integrals of j and j^2 are given by $2\pi h$ and $4h$, respectively. Since the surface resistance does not depend upon the surface location, the perimeter $2\pi r$ in Eqs. (6-7) and Eqs. (13-14) may be replaced with $4h$.

However, Y-C Chae has pointed out that the form factor for the longitudinal impedance in the limit case of a pair of parallel plates converges to unity [7]. Therefore,

$2\pi h$ may be used as an effective perimeter for the beam chamber. For this reason calculations for both perimeters are included in the Summary section.

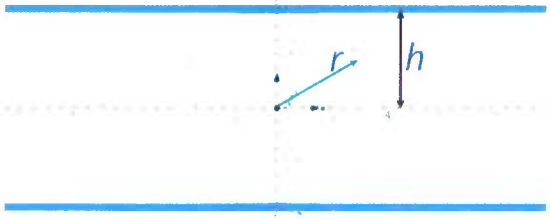

Fig. 1. The cross section of the rectangular beam chamber has half vertical aperture h. The effective perimeter for j was calculated to $2\pi h$, but that for j^2 was $4h$.

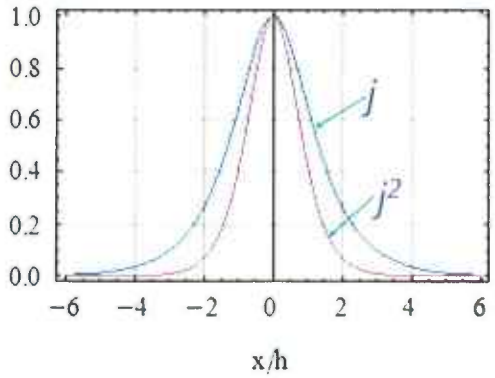

Fig. 2. Variations of the normalized current density j and density square j^2 as a function of x/h, where x is the distance in the horizontal direction from the density peak position.

6. Calculations

A few examples of the calculations for M = 24, a bunch length 0f 35 ps, and an average beam current of 0.1 A are shown graphically. Copper resistivity at 298 K, $(1/5.8)\times 10^{-7}$ Ωm, RRR = 1, was used as the reference. The harmonic coefficients are plotted in Fig. 3 to determine the harmonic numbers to be included in subsequent calculations. The parameter *alpha* determines which skin effect must be applied in Figures 4-8. Variations of the surface resistances (*Rs, Ras*) and heats loads (*dPsn, dPasn*) are plotted after applying for one or both normal (*Rs, dPsn*: *red curves*) and anomalous (*Ras, dPas: green curves*) skin effects.

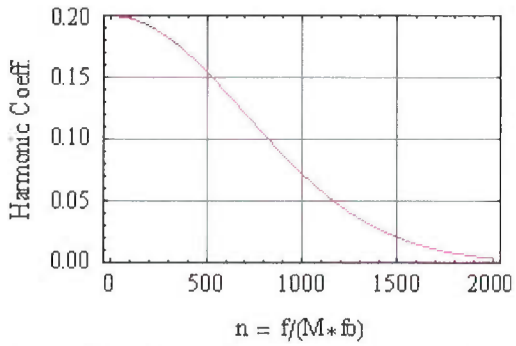

Fig. 3. Harmonic coefficients of Eq. (2) with I_{ab} = 0.1 A, M = 24, and bunch length of 35 ps are plotted as a function of the harmonic number n.

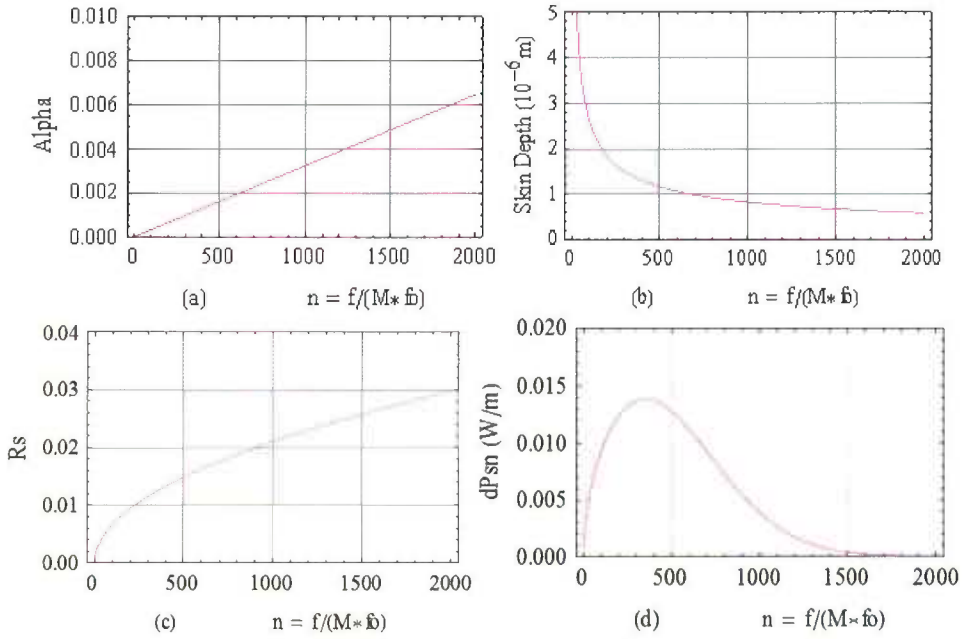

Fig. 4. For RRR = 1, variations of the alpha, skin depth, surface resistances, and heat loads are plotted as a function of the harmonics $n = f/(Mf_0)$. By applying the normal skin effect for alpha < 3, the calculated heat load per unit length from Eq. (6) or Eq. (7) was 10.77 W/m.

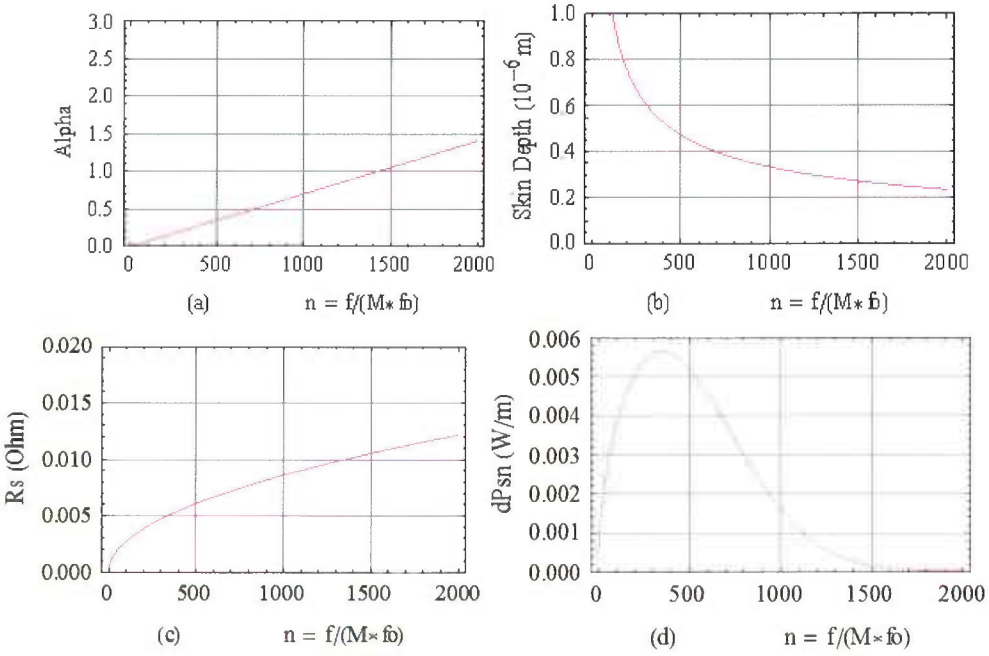

Fig. 5. For RRR = 6.16, variations of the alpha, skin depth, surface resistance, and heat load are plotted as a function of the harmonics $n = f/(Mf_0)$. By applying the normal skin effect for alpha < 3, the calculated heat load per unit length from Eq. (6) or Eq. (7) was 4.39 W/m.

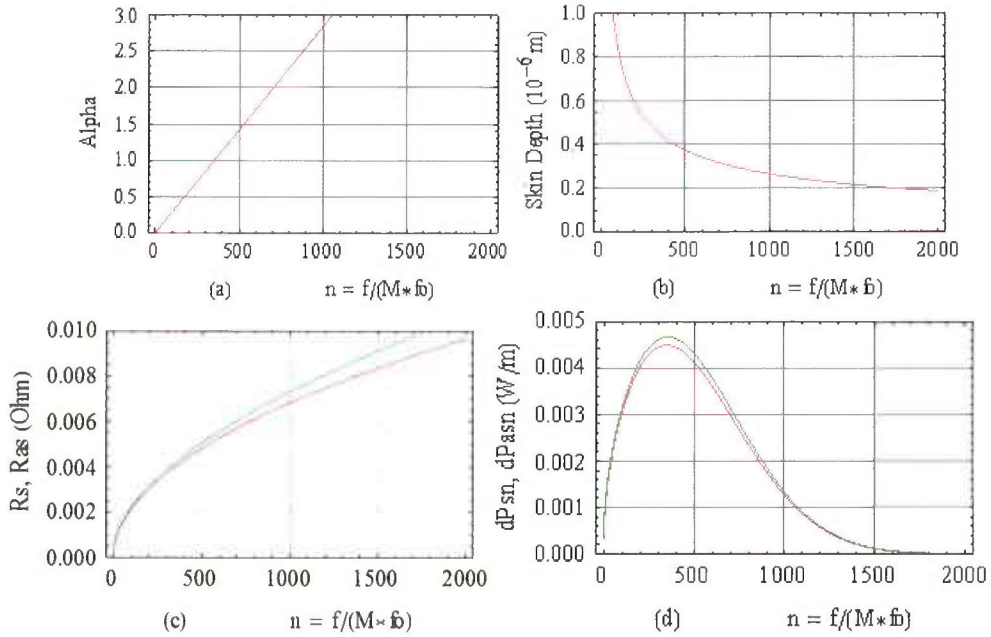

Fig. 6. For RRR = 10, variations of the alpha, skin depth, surface resistances, and heat loads are plotted as a function of the harmonics $n = f/(M f0)$. As shown in (a) the normal skin effect (*red curves*) was applied for $n < 1050$ and anomalous skin effect (*green curves*) for $n > 1050$. The calculated heat load per unit length was 3.50 W/m by using Eq. (7) and Eq (14) with adjusted summation limits.

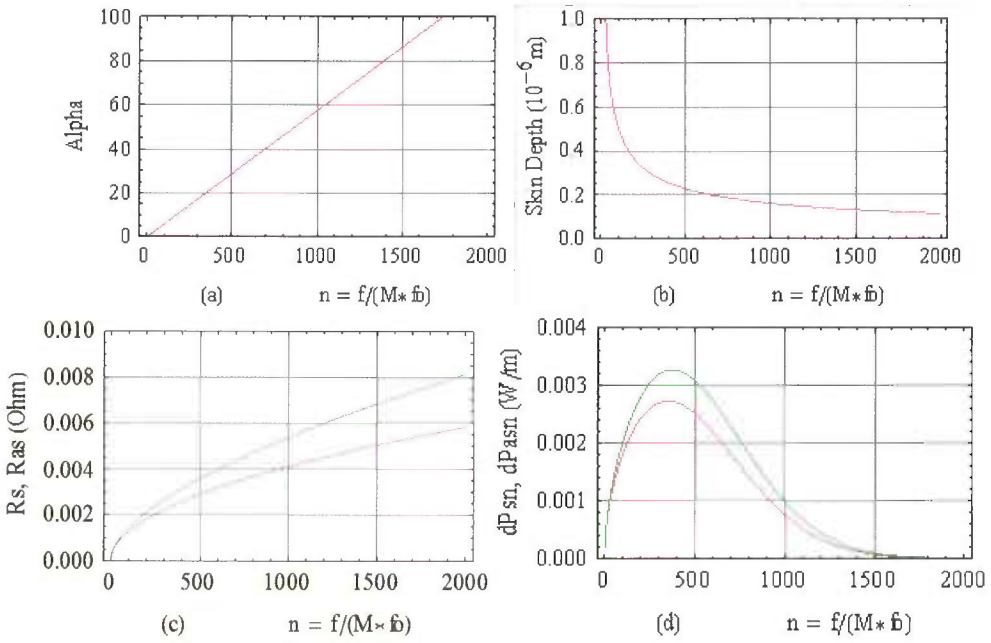

Fig. 7. For RRR = 30, variations of the alpha, skin depth, surface resistances, and heat loads are plotted as a function of the harmonics $n = f/(M f_0)$. By applying the anomalous skin effect (*green curves*) for alpha > 3, the calculated heat load per unit length was 2.57 W/m. By applying the anomalous skin effect *Ras* and consequently *dPasn* are higher than *Rs* (*red curve*) and consequently *dPsn* (*red curve*) for applying the normal skin effect.

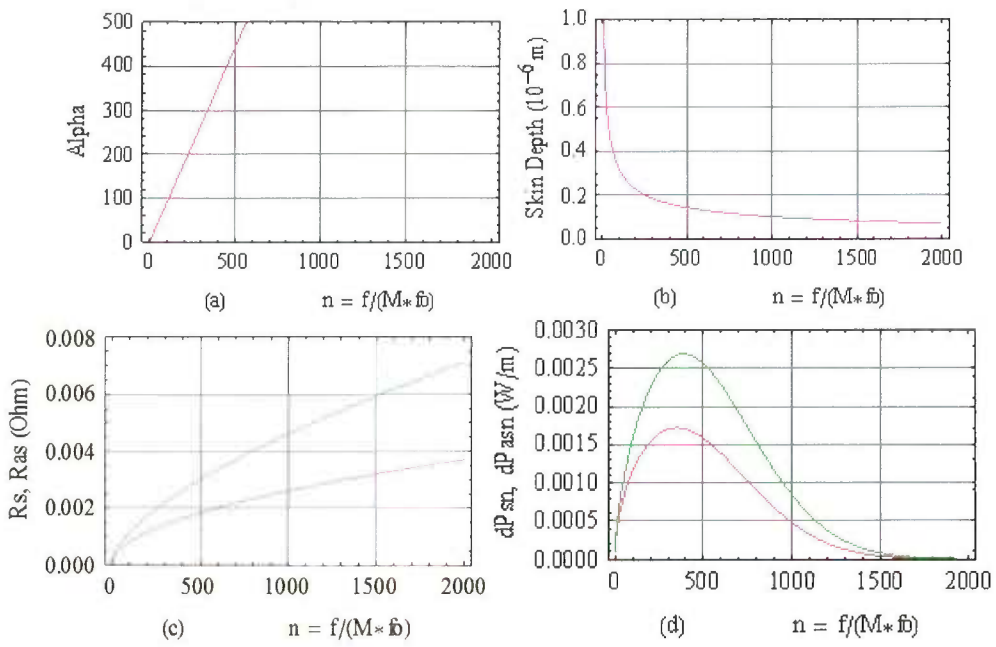

Fig. 8. For RRR = 100, variations of the alpha, skin depth, surface resistances, and heat loads are plotted as a function of the harmonics $n = f/(M f_0)$. By applying the anomalous skin effect (*green curves*) for alpha > 3, the calculated heat load per unit length was 2.13 W/m. By applying the anomalous skin effect *Ras* and consequently *dPasn* are higher than *Rs* (*red curve*) and consequently *dPsn* (*red curve*) for applying the normal skin effect.

7. Summary

From the calculations with the effective chamber perimeter of $4h$ the heat loads per unit length of the chamber are plotted as a function of RRR in Fig. 9. Copper resistivity, $(1/5.8) \times 10^{-7}$ Ωm at 298 K, has been used as the reference. RRRs of 8 and 80 correspond to the chamber temperature of about 80 K and 25 K, respectively. The normal skin effect was applicable for RRR < 9 and the anomalous skin effect was applicable for RRR > 25. In between the two RRRs both effects were used though the differences between the normal and anomalous effects were relatively small. Resistivity of the aluminum alloy 6063-T5 was about 2.8×10^{-9} Ωm at 20 K, while the RRR with respect to copper was about 6.16. The calculated heat loads for 6063-T5 in Fig. 9 are about 4.39 W/m for 35 ps and 0.1 A, and 12.34 W/m for 44.3 ps and 0.2 A.

The heat loads were also calculated assuming the effective chamber perimeter as $2\pi h$; the results are plotted in Fig. 10. The heat loads for 6063-T5 shown in the figure are about 2.80 W/m for 35 ps and 0.1 A, and 7.53 W/m for 44.3 ps and 0.2 A.

At a higher temperature of the 6063-T5 chamber at about 100 K the heat loads will be about twice those at 20 K. Decreasing the temperature below 20 K will not reduce the heat load because the 6063-T5 resistivity at 20 K is its minimum residual value. The figures also show that, because of the anomalous skin effect, even using a copper-coated chamber at RRR = 80 the heat loads will be reduced to only about 50% of the above calculations for the 6063-T5 chamber at 20 K.

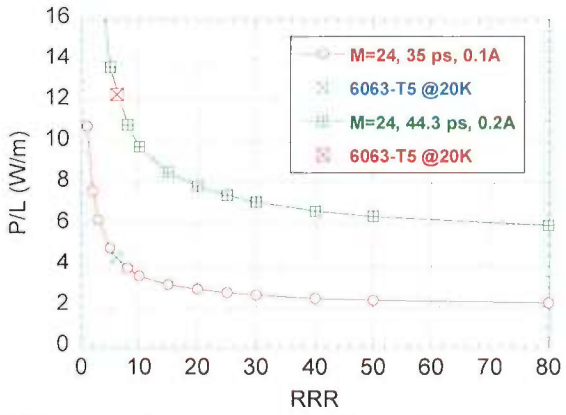

Fig. 9. Heat loads per unit length of the chamber with the effective chamber perimeter of $4h$ are plotted. For the aluminum alloy 6063-T5 at 20 K the heat loads were 4.39 W/m for 35 ps and 0.1 A, and 12.34 W/m for 44.3 ps and 0.2 A.

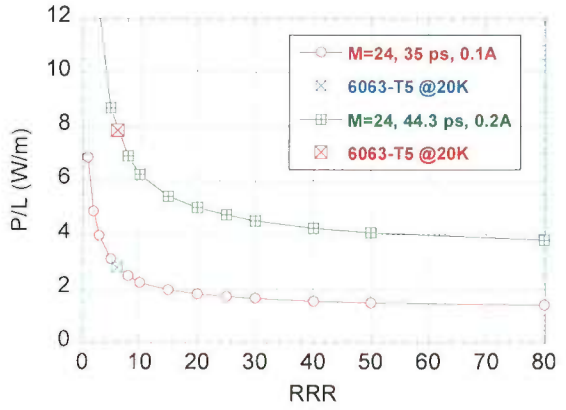

Fig. 10. Heat loads per unit length of the chamber with the effective chamber perimeter of $2\pi h$ are plotted. For the aluminum alloy 6063-T5 at 20 K the heat loads were 2.80 W/m for 35 ps and 0.1 A, and 7.85 W/m for 44.3 ps and 0.2 A.

References

[1] A.B. Pippard, "The Surface Impedance of Superconductors and Normal Metals at High Frequencies. II. The Anomalous Skin Effect in Normal Metals," Proc. Roy. Soc. London **A 191**, 385 (1947).

[2] G.E.H. Reuter and E.H. Sondheimer, "The Theory of the Anomalous Skin Effect in Metals," Proc. Roy. Soc. London **A 195**, 336 (1948).

[3] R.G. Chambers, "The Anomalous Skin Effect," Proc. Roy. Soc. London **A 215**, 481 (1952).

[4] W. Chou and F. Ruggiero, "Anomalous Skin Effect and Resistive Wall Heating," CERN LHC Project Note 2, 1995.

[5] R.L Powell, W.J. Hall, and H.M. Roder, "Low-Temperature Transport Properties of Commercial Metals and Alloys. II. Aluminums," J. Appl. Phys. **31**, 496 (1960).

[6] S.H. Kim, "Optimization of Four-Button BPM Configuration for Small-Gap Beam Chambers," BIW'98, AIP Conf. Proc. **451**, 310 (1998).

[7] L. Palumbo, V.G. Vaccaro, and M. Zobov, "Wake Fields and Impedance," CAS CERN Accelerator School, S. Turner, Ed., CERN 95-06, 1995.